High Temperature Oxidation Kinetics of Shot-Peened and Laser-Shock Peened Ti-Beta-21S

V. Optasanu, M. C. Marco de Lucas, A. Kanjer, B. Vincent, T. Montesin, L. Lavisse

High temperature oxidation kinetics of shot-peened and laser-shock peened Ti-Beta-21S

V. Optasanu, M. C. Marco de Lucas, A. Kanjer, B. Vincent, T. Montesin, L. Lavisse

Laboratoire Interdisciplinaire Carnot de Bourgogne, UMR 6303 CNRS - Université Bourgogne Franche-Comté, 9 Avenue A. Savary, BP 47 870, F-21078 Dijon Cedex, France

virgil.optasanu@u-bourgogne.fr; carmen.marco-de-lucas@u-bourgogne.fr; armand.kanjer@pandrol.com; benjamin_vincent@etu.u-bourgogne.fr; tony.montesin@u-bourgogne.fr; luc.lavisse@u-bourgogne.fr

Abstract. Isothermal oxidation tests of mechanically treated Ti-Beta-21S (TIMET, Ti-15Mo-3Nb-3Al-.2Si, ASTM Grade 21) were performed under dry air at 650, 700 and 750 °C during 100 h and compared to untreated samples. Two different mechanical surface treatments were used: Ultrasonic Shot-Peening (SP) and Laser-Shock Peening (LSP). The study investigates the effect of both treatments on the oxidation kinetics of the process and the role of atmospheric nitrogen insertion. With this aim, oxidation experiments were also performed under pure oxygen. The results show that the oxidation is governed by diffusion after a short transient time. Both SP and LSP treatments improve the high temperature oxidation resistance of Ti-Beta-21S in dry air, but not in pure oxygen. The formation of a nitrogen-enriched layer at the oxide-metal interface, which is promoted by the mechanical surface treatments, explains the increase of the oxidation resistance in air by slowing down the diffusion of oxygen into the metal.

Keywords Beta titanium metastable alloys, high temperature oxidation, diffusion, oxidation kinetics

Introduction

Advanced gas-turbine engines need new materials with excellent mechanical properties and resistance to high temperature (HT) oxidation. The combination of light-weight and good mechanical properties makes the titanium alloys very attractive to be used for compressor section components in gas turbine engines [1]. Titanium offers the potential for component weight savings of the order of up to 50 % compared to super alloys of Ni and steels. However, the mechanical properties of titanium deteriorate at HT due to both the growth of the oxide scale and the dissolution of oxygen into the metal lattice, which forms the so-called α-case. Both the oxide and the α-case are brittle materials and their formation must be limited.

Mechanical surface treatments such as shot-peening (SP), which can induce compressive stress and surface hardening, have shown their ability to improve the HT oxidation resistance of pure zirconium [2] and titanium [3] [4]. However, one of the side effects of SP treatments may be significant surface pollution caused by the balls used in the mechanical treatment. Laser-shock peening (LSP) appears as a good alternative to avoid this problem. Recently the use of LSP treatments has been reported to improve the HT oxidation resistance of pure (α-Ti) titanium [5] [4]. In our recent works we have shown that the LSP and SP treatment also increases the oxidation resistance of a Ti-Beta-21S, a metastable Ti-β alloy, for long exposure times, up to 3000 h [6] [7]. The LSP and SP samples showed 3 respectively 1.7 times less mass gain than the untreated material. The insertion of atmospheric nitrogen during the oxidation process appeared to be a key factor in the improvement of the oxidation resistance. The insertion of nitrogen at the interface between the oxide and the metal was also observed by Dupressoire et al. [8] and Berthaud et al. [9] on Ti6242S alloy.

The influence of the surface mechanical treatments cannot persist for a long time at high temperatures because of the thermal effects: defects recovering, annealing, recrystallization and grain growth. Thus, the differences remarked in long oxidation tests [6] [7], can only be explained by differences in the early stages of the oxidation process. The titanium oxides are thermodynamically more stable than nitrides. The formation of nitrides shows that they are promoted by the kinetics of reaction at the early stages of the high temperature exposure, when the structural modifications induced by the surface mechanical treatment are still present.

As the changes in the microstructure made by the mechanical treatments (SP and LSP) are rapidly annihilated at high temperature, the large differences in the mass gain measures after 3000 h of exposure at high temperature can only be explained by the differences of mechanisms at the beginning of the oxidation process. In the present work, we investigate the oxidation kinetics of Ti-Beta-21S in the first stages of the high temperature oxidation process in air and how SP and LSP treatments change it. For this, the mass gain was recorded as a function of time up to 100 h by thermogravimetric analysis (TGA) at different temperatures: 650, 700 and 750 °C. Untreated samples (US) were also studied for comparison. The variation of the mass gain as a function of time was analyzed using a complete parabolic law [10]. In order to investigate the insertion of atmospheric nitrogen during HT

oxidation and the effect of the SP and LSP treatments on this process, HT oxidation experiments were also performed under pure oxygen at 700 °C. Cross-sections of oxidized samples were analyzed by scanning electron microscopy (SEM) coupled to energy-dispersive spectroscopy (EDS), electron backscattered diffraction (EBSD). X-ray photoelectron spectroscopy (XPS), X-ray diffraction (XRD), and micro-Raman spectroscopy were also used for surface analysis of the samples.

Experimental methods

The Titanium Ti-Beta-21S metastable (TIMET supplier) was used in this study. Its chemical composition (wt. %) is: Ti 78, Mo 15.13, Nb 2.65, Fe 0.26, Si 0.2, Al 3.45, C 0.013, O 0.13, N 0.02. For mechanical pretreatments, samples of 25 x 50 x 1.8 mm^3 were cut from plates produced by TIMET. High temperature oxidation (HT) experiments were performed on samples of 10 x 10 x 1.8 mm^3. Mechanical treatment details are given in previous work [4]. In summary, the SP treatment was made with WC balls (20 g of 2 mm diameter balls) vibrated at 20 kHz with 15 µm of amplitude. The LSP treatment used a GAIA HP laser source at 532 nm (duration of the laser shots: 7 ns, frequency: 0.5 Hz, diameter of the focal spot: 4 mm, overlap of shots: 30%). The deposited laser irradiance was 9.1 GW/cm^2. An aluminum foil tape was used as a thermal protection of the samples during the LSP treatment under water [11].

Oxidation experiments were performed by isothermal exposure in a thermogravimetric analyzer (TGA) SETARAM SETSYS EVOLUTION 1750 under either dry synthetic air or pure oxygen at a constant flow of 20 mL/min. The temperatures investigated here were 650, 700 and 750 °C. A heating rate of 10 °C/min was used from ambient temperature up to 10 °C under the target temperature, and then the heating rate was reduced to 1 °C/min.

X-ray diffraction phase analysis was carried out by using a BRUKER D8-A25 DISCOVER diffractometer. A Cu anticathode was used with a fix beam incidence of 2°. Micro-Raman spectroscopy analysis was done with a Renishaw InVia set-up in backscattering configuration. The wavelength used was 532 nm and the excitation power focused on the sample was about 0.5 mW to avoid heating. The chemical state of the samples before oxidation and after 5h of exposure at 700 °C in dry air was analyzed by XPS (PHI Versaprobe 5000). Before analysis, the sample surface was cleaned by bombardment with argon ion beam (Ar^+) at 5 keV for 1 min.

After oxidation, the samples were cross-sectioned, resin-embedded and mirror polished up to 50 nm colloidal silica suspension. Cross-sections of the samples were analyzed by SEM coupled to an electron microprobe in order to investigate the distribution of the alloying elements. Two microscopes coupled to energy-dispersive spectroscopy (EDS) probes were used here, a TESCAN VEGA 3 and a field-emission microscope JEOL JSM-7600F. The grain orientation was characterized by EBSD (TSL EDAX OIM X4M EBSD system) coupled with the JEOL-7600F microscope. The working distance was 20 mm, the tension 20 kV, the magnification x70 and the scanning step was 1 µm.

Results and discussion

Microstructure before oxidation

Figure 1 displays SEM images of three samples cross-section before oxidation: US, SP and LSP. The samples surface is located on the upper part of the images. The images display significant differences in the microstructure depending on the treatment. The SP samples (Fig.1b) display a large number of slip planes and a significant sub-grain nanostructuration about 100 µm under the samples' surface. In the LSP samples (Fig.1c) the appearance of a network of twins mainly near the grain boundaries can be observed.

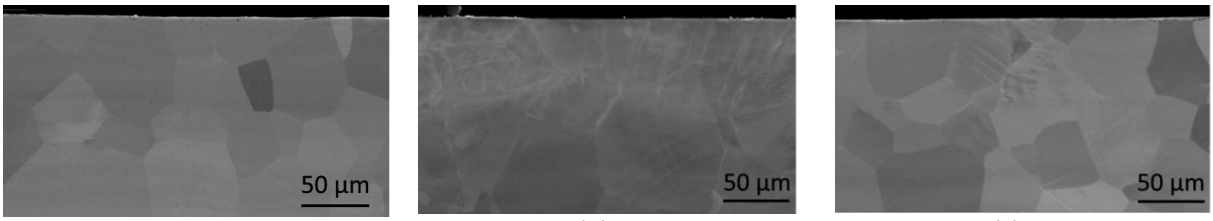

Fig. 1. Cross section SEM images (in BSE mode) of untreated (a), shot peened (b) and laser-shock peened (c) samples.

The analysis of treated and untreated samples by XRD showed mainly the beta-Ti phase. For LSP treated samples, it was recently shown that the treatment induces the formation of a small amount of the martensitic α'' phase [6]. The analysis by XPS showed a slight surface oxidation of LSP treated samples where the presence of alumina, molybdenum oxide and sub-stoichiometric titanium dioxide was identified. For SP treated samples, the analysis by Raman spectroscopy revealed the presence of tungsten carbide particles on top of the sample surface, coming from the balls used for the SP treatment.

Kinetic analysis of HT exposure in air and pure oxygen

Isothermal oxidation experiments using TGA allow recording of a quasi-continuous variation of the mass gain as a function of the HT exposure time. The evolution of the mass gain per unit area at 700 °C in dry air during 100 h is shown for the US, SP and LSP samples in Figure 2a. For untreated samples the total mass gain after 100 h was similar to that reported by Wallace et al. [12]. For SP and LSP treated samples the mass gain is smaller compared to US samples. The effect is higher for SP samples for short oxidation times, but the mass gain is almost the same for SP and LSP samples after 100 h of exposure at 700 °C. According to the slope of the variation of the mass gain, the LSP treatment would provide a better protection against oxidation for longer exposure time to HT. This was confirmed in a previous work for long exposure (3000 h) to HT [6]. The same effect was also reported by Kanjer *et al.* [4] for pure Ti.

The XRD analysis performed on samples oxidizer for 5h at 700°C showed the presence of alpha phase of Ti, small peaks of alumina and the presence of anatase along the main phases which are the rutile and the beta titanium. Behera et al. [13] obtained similar results. As expected, the oxygen dissolution in the metal promotes the beta to alpha phase transformation.

The classical Wagner theory [14] shows that, if the oxidation is governed by the diffusion, the variation of the mass gain with time can be expressed as a pure parabolic function:

$$\Delta m^2 = k_p\, t \qquad (1)$$

where Δm is the mass gain per unit area at time t and k_p is the parabolic rate constant.

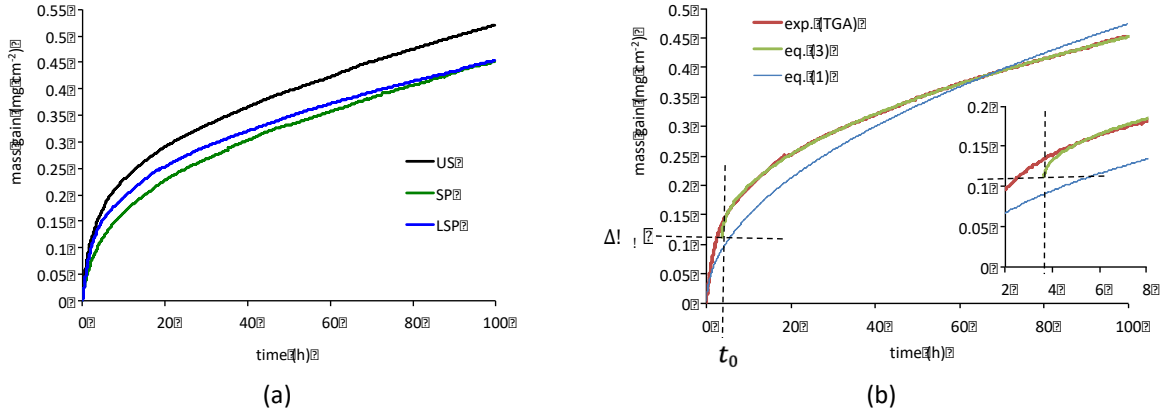

Fig. 2. (a) Mass gain per unit area as a function of the oxidation time measured by TGA during 100 h of exposure at 700 °C in dry air for Ti-Beta-21S US, SP and LSP samples. (b) Experimental mass gain versus time for the LSP sample at 700 °C in air (red), fit with a complete parabolic function (eq. 3) (green), and with a pure parabolic function (eq. 1) (blue).

In practice, the mass gain is rarely purely parabolic such as eq. (1) describes, especially at the beginning of oxidation, due to the presence of an initial oxide layer, microstructural changes, or slow oxidation reactions. If oxidation is governed by diffusion after a transient time, then it is possible to fit the mass gain versus time curve with a complete parabolic function [10]:

$$t = A + B\,\Delta m + C\,\Delta m^2 \qquad (2)$$

This expression can be rewritten as follows:

$$(\Delta m - \Delta m_0)^2 = k_p (t - t_0) \qquad (3)$$

where Δm_0 and t_0 are the coordinates of the origin of a pure parabolic function, and k_p (eq. 3) is the parabolic rate constant. This can be seen as an offset (change of coordinates) that transforms the complete parabolic function (eq. 2) into a pure parabolic law (eq. 3). The couple (Δm_0, t_0) represents the coordinates of the origin of a pure parabolic function: Δm_0 is the oxide mass gain per unit area at time t_0 and t_0 is the corresponding initial time of the pure parabolic behaviour. The values of Δm_0, t_0 and k_p can be found by fitting the experimental curve to eq. (3) for $t > t_0$ using the least squares method. Several iterations are made to obtain the best fit of the experimental curve from $t = t_0$ up to $t = 100$ h. At each iteration, a new couple of values Δm_0 and t_0, is estimated. This iterative process ends when the values of Δm_0 and t_0 remain steady.

The Figure 2b shows two different parabolic fits: one with a complete parabolic function (green line obtained with eq. 3) and the other with a pure parabolic function (eq. 1). A simple parabolic law, eq. (1), used to fit the whole curve, gives quite a bad approximation (blue curve, Fig. 2b). As expected, the complete parabolic law fits the experimental mass gains curve (green curve, Fig. 2b) the best by far. One can see then that the mass gain is described by a complete parabolic expression (eq. 3) with the condition to consider a transient period, given by (Δm_0, t_0) when the mass gain is not parabolic. This proves that during the transient period ($t < t_0$) the diffusion is not the main mechanism governing the oxidation, but after this transient period the oxidation is driven by the diffusion mainly.

Table 1 shows the values of Δm_0, t_0 and the parabolic constant k_p obtained by fitting the experimental curves obtained for US, SP and LSP samples at different temperatures. As expected, the longest transient time t_0, is found for the lowest temperature (650 °C), while it is the shortest at 750 °C. This shows that the phenomena involved in the transient time t_0 are thermally activated. Moreover, one can clearly see that the biggest value of t_0 is obtained for the SP samples at 650 °C. This can be explained by the fact that the shot-peened samples have suffered the most important microstructural modifications as seen in Figure 1. The mechanical history of SP samples disappears only after 12 h. On the contrary, at the highest temperature (750 °C) the microstructural modifications introduced by the SP treatment are not present anymore, which can be explained by the recrystallization of the nanostructured sample microstructure during the heating ramp. This recrystallization is probably accelerated by the high amounts of elastic energy density stored into the material. Kanjer *et al.* [3] have noticed, in the mechanically affected area of the shot-peened pure Ti samples, larger grains after oxidation compared with untreated samples, which suggest that the recrystallization was accelerated by the nanocristallization and the mechanical energy stored into the material.

As expected the parabolic rate constant, k_p, (Table 1) increases with the temperature. Moreover, the values corresponding to SP and LSP samples are smaller than those of the US sample. In addition, one can see the apparent anomalous behavior of the SP samples for which parabolic rate constant do not regularly evolve. Thus, at the lowest temperature, 650 °C, the parabolic rate constant value is very close to the LSP one. Then at 700 °C, the LSP parabolic rate constant value is significantly smaller than the SP one (25 % less) but their values become close at 750 °C. The formation of the oxide scale seems to be different for the two types of mechanical treatments.

Table 1. Parameters optimizing the fit of the experimental masse gain curves versus time to eq. (3): initial mass gain per unit area Δm_0 (10^{-2} mg cm^{-2}), time t_0 (h) and the parabolic rate constant, k_P (10^{-6} mg^2 cm^{-4} s^{-1}).

	650 °C			700 °C			750 °C		
	Δm_0	t_0	k_p	Δm_0	t_0	k_p	Δm_0	t_0	k_p
US	0.05	7.0	0.13	0.11	2.0	0.47	0.04	0.8	1.7
SP	0.07	12.0	0.10	0.06	2.0	0.44	0.01	0.2	1.5
LSP	0.04	6.6	0.10	0.11	3.7	0.33	0.03	2.0	1.6

The activation energy of the oxidation process, E_a, was calculated using the Arrhenius's fit method. The value obtained for untreated Ti-Beta-21S was about 200 kJ.mol^{-1}, which is close to the activation energy of 180 kJ.mol^{-1} reported by Chaze and Coddet [15] for pure titanium. Moreover, the addition of alloying elements such as Al and Si was reported to increase the activation energy. Here, for SP and LSP treated samples of Ti-Beta-21S the activation energy obtained by the Arrhenius's fit method was about 215 kJ.mol^{-1}. So, both mechanical treatments lead to a small increase of the activation energy of the oxidation process of Ti-Beta-21S.

A closer look at the beginning of the oxidation process can show how the diffusional process evolves with time. We proceed to calculate the instantaneous parabolic constant, as defined by Monceau and Pierragi [10] with a moving window width of 2.5 h (Fig. 3). At 700 °C in air, the SP sample presents the smallest variation of k_p, while the untreated and LSP samples present a continuously decreasing value of the parabolic constant k_p. This suggests that the highly nanostructured surface of SP samples influences the first stages of the oxidation.

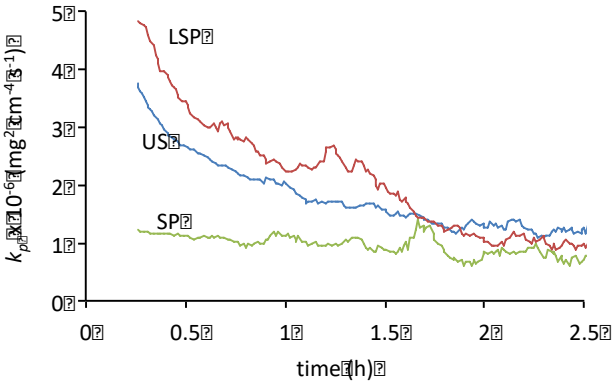

Fig 3. Instantaneous parabolic rate constant, k_P, in the first stages of oxidation under dry air at 700 °C.

It has been reported that the SP treatment activates nitriding [16] [17]. The penetration of large quantities of nitrogen at the first stages of oxidation could explain the slowing down of the oxidation rate. In fact, the atoms of nitrogen occupy the same interstitial octahedral sites [18] as oxygen ones. Thus, the insertion of nitrogen can reduce the mobility of oxygen. The oxidation tests in air reported by Chaze and Coddet [15] showed the important role of nitrogen. Moreover, we have recently demonstrated that nitrogen is present in larger quantities in oxidized samples of LSP treated Ti-Beta-21S compared to untreated samples for long exposures to high temperature [6]. The insertion of nitrogen at the metal-oxide interface improves the HT oxidation resistance of Ti-Beta-21S in a

similar way to that of pure titanium [4], they are both impacted positively by the presence of nitrogen at the interface oxide/metal.

In order to analyse the influence of nitrogen on the oxidation process, isothermal oxidation experiments under pure oxygen were done recording the variation of the mass gain per unit area by TGA. Figure 4 displays the variation of the mass gain per unit area during the exposure at 700 °C in pure oxygen. The variation of the mass gain as a function of time showed for the three kinds of samples (US, SP and LSP) a pure parabolic behavior up to about 10 h, which is followed by a quasi-linear variation from 10 h up to 100 h at 700 °C. This linear behavior suggests that the oxide scale is not protective anymore against the oxidation at this stage. The formation of cracks occurs in the oxide layer. The stratification of the oxidation layer can be seen in cross-section SEM images that will be discussed further in this paper.

The very first stages of oxidation (< 10 h) in pure oxygen show a similar mass gain variation for untreated and SP and LSP treated samples. In opposition, in air atmosphere, the mass gain was affected by the mechanical treatment of the samples. This demonstrates the important role of atmospheric nitrogen for explaining the higher oxidation resistance of SP and LSP treated Ti-Beta-21S in dry air (Fig. 2). The high density of grain boundaries and defects induced by the mechanical treatments (Fig. 1), mainly in the case of the SP treatment, enhances the diffusion of nitrogen and promotes the formation of a nitrogen-enriched layer at the oxide-metal interface. This effect was shown for LSP samples of Ti-Beta-21S after oxidation during long exposure (3000 h) at 700 °C [6]. The same behavior was observed by Kanjer *et al.* for pure Titanium [3] [5] [4].

The k_P values calculated using the complete parabolic expression for pure oxygen atmosphere on the first 10 h of oxidation are given in Table 2 together with the average k_p values obtained in the same time range for oxidation under dry air. One can observe that under pure oxygen the values of the parabolic rate constant are close between US, SP and LSP. These values are much bigger than those obtained in dry air. Moreover, the US sample shows the lowest k_P value, which is consistent with the fact that the reference samples present fewer defects and no nanostructuration. The SP samples display the highest parabolic rate. This is consistent with the presence of the highest density of defects and grain boundaries (Fig. 1), which can act as preferential short-cuts for the diffusion of oxygen. Conversely, under air, the untreated samples showed the highest average oxidation rate, which suggests that the defects in LSP and particularly in SP samples slow down the oxidation rate in presence of nitrogen. This confirms the significant role of nitrogen in the high temperature oxidation kinetic of mechanically treated Ti-Beta-21S under air.

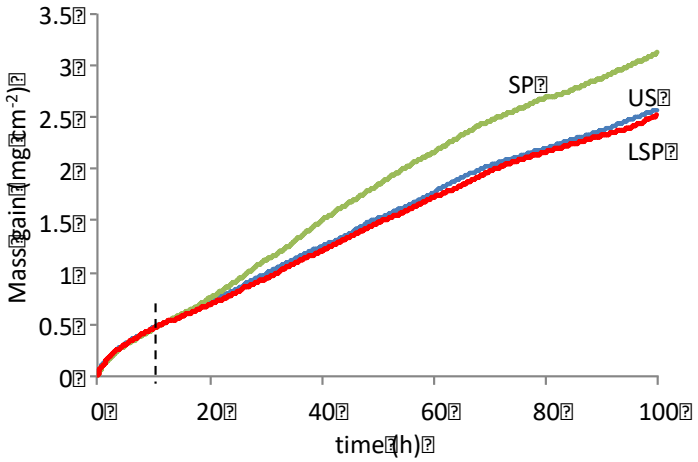

Fig. 4. Mass gain per unit area as a function of the time in pure oxygen at 700 °C for US, SP and LSP samples.

Table 2. Parabolic rate constant, k_p (10^{-6} mg².cm^{-4}.s^{-1}), obtained by fitting to a complete parabolic law the mass gain per unit area as a function of the time up to 100 h for US, SP and LSP samples at 700 °C in dry air and in pure oxygen.

	k_p (10^{-6} mg² cm^{-4} s^{-1})		
	US	**SP**	**LSP**
Pure O_2	7.4	8.3	7.7
Dry air	1.30	0.69	0.73

Microstructure after oxidation

Figure 5 displays EBSD maps on cross-sections of SP samples after oxidation during 5 h at 700 °C. It shows the distribution of β-Ti phase (in green) and α-Ti phase (in red) in the metal under the oxide layer. The strongest effect is observed in the SP sample where about 2.5 % of β-Ti has been transformed into α-Ti. The α-Ti phase is mainly formed along the grain boundaries up to about 100 µm under the surface. As SP treatment promotes nanostructuration, it increases the diffusion paths and promotes the diffusion of the oxygen and nitrogen, which are alpha-stabilizing elements. Wen and al [19] [20] reported sensible increase of the length of diffusion for O, N, and C after one hour of exposure at 700 °C in air. The fraction of α-Ti phase is lower than 1 % in 5 h oxidized US

and LSP samples. Guttmann [21] proposed that the stress generation combined with plastic deformation induced by the SP treatment induces grain refinement and higher substrate reactivity due to the increase of surface energy induced by the SP treatment.

SEM cross-section images of samples oxidized for 100 h in dry air and in pure oxygen are shown in Figures 6 and 7, respectively, for an untreated sample (US) and two mechanically treated samples, SP and LSP. Elemental maps showing the spatial distribution of Ti, Al, O and N obtained by EDS are also shown. One clearly observes that, as expected, the oxide scale is much thicker in pure oxygen than in air. In the first case, a stratified oxide scale is formed for all the samples as previously reported by Dechamps et al. [22].

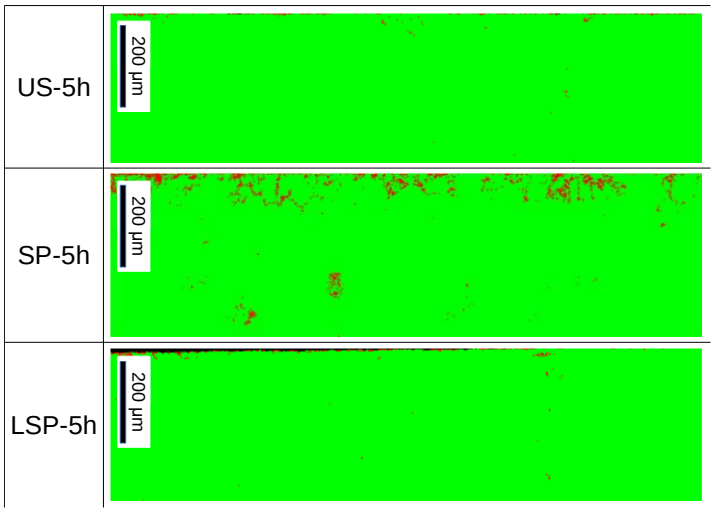

Fig. 5. Results of analysis by EBSD of the cross-section of oxidized US, SP and LSP showing the distribution of β-Ti (in green) and α-Ti (in red) phases. The samples were oxidized during 5 h at 700 °C in dry air. The top of the maps corresponds to the oxide-metal interface.

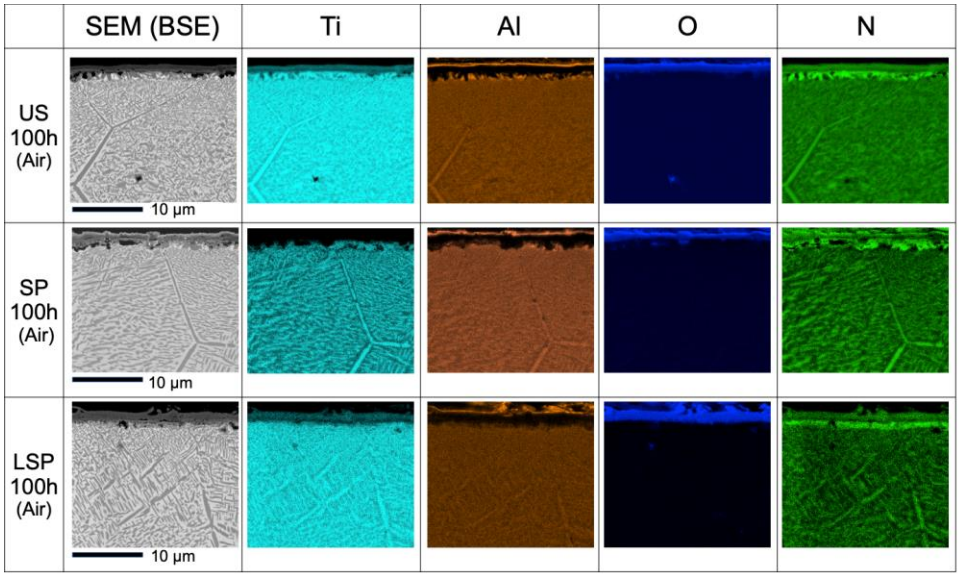

Fig. 6. EDS cross-section cartographies of US, SP and LSP samples exposed during 100 h at 700 °C in dry air.

The first observation that can be made is that in dry air the thinnest oxide layer is exhibited by the US sample compared with SP and LSP. We saw earlier that, on the contrary, the mass gain during the oxidation is bigger for US than for SP and LSP. Thus, the quantity of oxygen in solid solution in the metal must then be larger in US than in SP and LSP. This is consistent with the observations made by Ion Beam Analysis for untreated and LSP samples of Ti-Beta-21S for long oxidation durations [6]. In the same work we showed that the quantity of nitrogen under the oxide scale is bigger in LSP than in US samples and that the extent of the nitrogen-enriched zone is larger for LSP. The nitrogen is rather difficult to quantify with EDS techniques in presence of titanium since the L peak of titanium and the K peak of nitrogen are close, which makes their deconvolution difficult. However, on the EDS maps of nitrogen presented in Figure 6 one can clearly observe that the extent of the nitrogen-enriched zone under the oxide scale is thicker for SP than US (and even than LSP). The same conclusion can be drawn by observing the SEM image taken in BSE mode (which displays the chemical contrast) where a larger medium grey zone can

be observed just under the oxide scale of the SP sample compared to US. The larger amounts of nitrogen under the oxide scale of the SP and LSP sample is probably the origin of the lower mass intake of oxygen during the oxidation because it slows down the oxygen diffusion into the Ti lattice. This nitrogen-enriched layer was previously observed in the case of pure titanium for the same kind of treatments, SP and LSP [4].

The diffusion coefficients of oxygen and nitrogen in β-Ti are barely known in the temperature range studied in this work. They have been reported only at higher temperatures in ref. [23]. Both oxygen and nitrogen promote the β-Ti to α-Ti transition, but the solubility of nitrogen in titanium is smaller than that of oxygen. In α-Ti, the diffusion coefficient of oxygen at 700 °C is almost a hundred times that of nitrogen [23] [24] [25] [26]. As a consequence for HT oxidation in air, the diffusion of nitrogen through the oxide-metal interface is very small compared to oxygen, which can explain the formation of a nitrogen-enriched layer at this interface. Once formed, this layer makes more difficult the diffusion of oxygen into the metal because both nitrogen and oxygen atoms occupy the same kind of interstitial sites in the structure of titanium.

The EDS maps also show the presence of Al, probably forming an alumina layer, on the top of each stratum of the oxide scale for all the samples (air and pure oxygen atmospheres). This agrees with the observations reported for longer exposure times [6] and can be explained by its bigger thermodynamic stability compared to rutile.

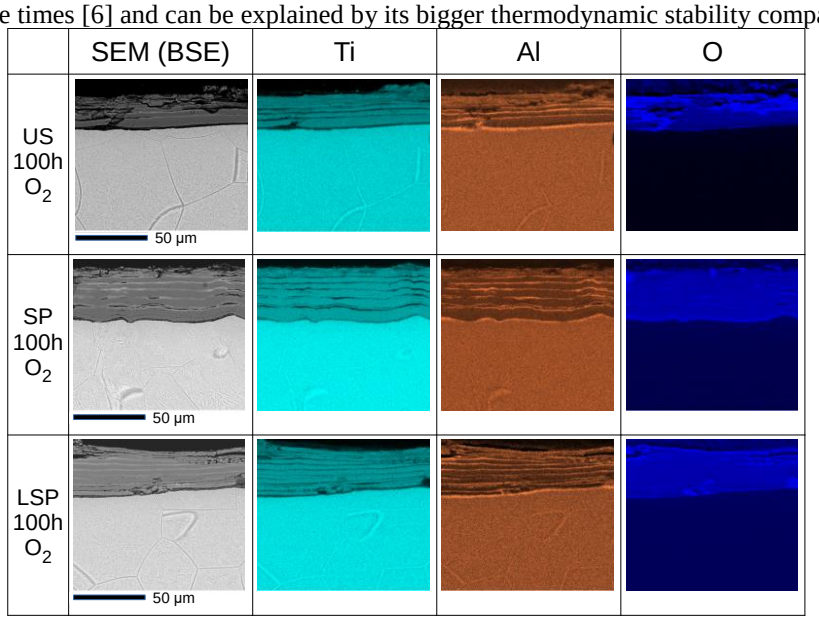

Fig. 7. EDS cross-section cartographies of US, SP and LSP samples exposed during 100 h at 700 °C in pure oxygen.

Nuclear reactions analysis combined with XRD and XPS showed that the nitrogen is still present after 3000 h at the interface between the oxide and the metal [6], which indicates that the nitrogen finds favorable thermodynamic conditions to form stable compounds. Abdallah et al. [27] have also shown the presence of oxynitrides, Ti_2N and TiN in samples oxidized for 100 h at 650 °C.

Conclusion

The isothermal oxidation kinetics of the β-metastable Ti-Beta-21S alloy has been studied during 100 h in dry air in the 650- 750 °C range. The effects of two mechanical treatments, shot peening (SP) and laser shock penning (LSP), have been studied. Moreover, thermogravimetric analyses at 700 °C under pure oxygen were also done in order to investigate the role of atmospheric nitrogen in the high temperature oxidation process.

The microstructural analysis by SEM on cross-sections of SP treated samples revealed a high density of defects and nanostructuration, while LSP samples shows some networks of twins.

Both mechanical treatments induced a reduction of the mass gain by oxidation in air during 100 h. The analysis of the variation of the mass gain as a function of the time showed a parabolic behaviour after a short transient time, which shows that oxidation is governed by the diffusion of oxygen.

For oxidation in pure oxygen, the variation of the mass gain displays a pure parabolic behaviour up to about 10 h. No significant difference was observed between untreated and treated samples. For longer times, the oxidation scale becomes strongly stratified and the mass gain variation becomes almost linear. SP treated samples display a higher oxidation rate than US and LSP samples. This demonstrates the significant role of atmospheric nitrogen in the HT oxidation of Ti-Beta-21S in air and show that the nitrogen insertion is influenced by the mechanical surface treatments, which leads to modification of the kinetics of oxidation.

The cross-section analysis of oxidized samples by EDS suggests the formation of a nitrogen-enriched layer at the oxide-metal interface. The presence of titanium oxynitrides was already shown by XRD analysis for LSP treatments after 3000 h of exposure [6]. These results show that the insertion of nitrogen at the oxide-metal interface, which was reported in previous works for samples oxidized during long durations, takes place at the very first stages of the oxidation process. The smaller diffusion coefficient of nitrogen compared to oxygen would

explain the formation of this nitrogen-enriched layer. Once formed, it would act as a brake for the diffusion of oxygen through the oxide-metal interface. The defects induced by mechanical surface treatments promote the insertion of larger amounts of nitrogen. These combined effects would explain the higher oxidation resistance of SP and LSP treated Ti-Beta-21S in air.

Acknowledgements
Authors acknowledge greatly Burgundy Regional Council (BRC) and the Agglomeration Council of Chalon City for their financial contribution in SEM at Chalon sur Saône, and the PIMM Laboratory (HESAM University) and the Charles Delaunay Institute (University of Technology of Troyes) for the mechanical treatments. This work was supported by the EIPHI Graduate School (contract ANR17-EURE-0002).

References

[1] J.C. Williams and E.A. Starke, *Acta Materialia*, vol. 51, pp. 5775-5799, 2003.

[2] L. Raceanu, V. Optasanu, T. Montesin, G. Montay, and M. François, *Oxidation of metals*, vol. 79, no. 1-2, pp. 135-145, 2013.

[3] A. Kanjer et al., *Surface and Coatings Technology*, vol. 343, pp. 93-100, 2018.

[4] A. Kanjer et al., *Oxidation of Metals*, vol. 88, no. 3-4, pp. 383-395, 2017.

[5] A. Kanjer et al., *Surface and Coatings Technology*, vol. 326, pp. 146-155, 2017.

[6] L. Lavisse et al., *Surface and Coating Technology*, vol. 403, p. 126368, 2020.

[7] L. Lavisse et al., in *The 14th World Conference on Titanium*, vol. 321, 2020, p. 04001.

[8] C. Dupressoire et al., *Oxidation of Metals*, vol. 87, no. 3-4, pp. 343-353, 2017.

[9] M. Berthaud et al., *Corrosion Science*, vol. 164, p. 108049, 2020.

[10] D. Monceau and B. Pieraggi, *Oxidation of metals*, vol. 50, no. 5-6, pp. 477-493, 1998.

[11] P. Peyre, R. Fabbro, P. Merrien, and H. P. Lieurade, *Materials Science and Engineering A*, vol. 210, pp. 102-113, 1996.

[12] T. A. Wallace, R. K. Clark, and K. E. Wiedemann, in *NASA Technical Memorandum 104217*, Hampton, VA (United States), Langley Res., 1992.

[13] A. Behera et al., *Journal of Materials Science*, vol. 48, pp. 6700–6706, 2013.

[14] P. Kofstad, *High temperature corrosion*.: Elsevier Applied Science Publishers Ltd., 1988.

[15] A.M. Chaze and C. Coddet, *Journal of the Less Common Metals*, vol. 124, no. 1-2, pp. 73-84, 1986.

[16] S. M. Hassani-Gangaraj, A. Moridi, M. Guagliano, A. Ghidini, and M. Boniardi, *International Journal of Fatigue*, vol. 62, pp. 67-76, 2014.

[17] O. Unal, E. Maleki, and R. Varol, *Vacuum*, vol. 150, pp. 69-78, 2018.

[18] T. Tsuji, *Journal of Nuclear Materials*, vol. 247, pp. 63-71, 1997.

[19] M. Wen, C. Wen, P. Hodgson, and Y. Li, *Colloids and Surface B: Biointerfaces*, vol. 114, pp. 658-665, 2014.

[20] M. Wen, C. Wen, P. Hodgson, and Y. Li, *Corrosion Science*, vol. 59, pp. 352-359, 2012.

[21] E.M. Gutmann, *Mechanochemistry of solid surfaces*.: Edition World Scientific Pub. Co., 1994.

[22] M. Dechamps, J. Desmaison, and P. Lefort, *Journal of the Less Common Metals*, vol. 71, no. 2, pp. 177-181, 1980.

[23] C. Zeng, H. Wen, B. Zhang, P. T. Sprunger, and S. M. Guo, *Applied Surface Science*, vol. 505, p. 144578, 2020.

[24] A. Antilla, J. Raisanen, and J. Keinonen, *Applied Physics Letters*, vol. 42, no. 6, pp. 498-500, 1983.

[25] D. David, G. Beranger, and E. A. Garcia, *Journal of The Electrochemical Society*, vol. 130, no. 6, pp. 1423-1426, 1983.

[26] Z. Liu and G. Welsch, *Metallurgical Transactions A*, vol. 19A, pp. 1121-1125, 1988.

[27] I. Abdallah, C. Dupressoire, L. Laffont, D. Monceau, and A.V. Put, *Corrosion Science*, vol. 153, pp. 191-199, june 2019.